metals

MDPI

Article

Influence of Shot Peening on the Isothermal Fatigue Behavior of the Gamma Titanium Aluminide Ti-48Al-2Cr-2Nb at 750 °C

Christoph Breuner [1,*], Stefan Guth [1], Elias Gall [1], Radosław Swadźba [2], Jens Gibmeier [1] and Martin Heilmaier [1]

[1] Karlsruhe Institute of Technology, IAM-WK Institute for Applied Materials, Engelbert-Arnold-Straße 4, 76131 Karlsruhe, Germany; stefan.guth@kit.edu (S.G.); uoftr@student.kit.edu (E.G.); jens.gibmeier@kit.edu (J.G.); martin.heilmaier@kit.edu (M.H.)

[2] Łukasiewicz Research Network, Institute for Ferrous Metallurgy, K. Miarki 12-14, 44-100 Gliwice, Poland; Radoslaw.Swadzba@imz.lukasiewicz.gov.pl

* Correspondence: Christoph.Breuner@kit.edu; Tel.: +49-721-608-47446

Abstract: One possibility to improve the fatigue life and strength of metallic materials is shot peening. However, at elevated temperatures, the induced residual stresses may relax. To investigate the influence of shot peening on high-temperature fatigue behavior, isothermal fatigue tests were conducted on shot-peened and untreated samples of gamma TiAl 48-2-2 at 750 °C in air. The shot-peened material was characterized using EBSD, microhardness, and residual stress analyses. Shot peening leads to a significant increase in surface hardness and high compressive residual stresses near the surface. Both effects may have a positive influence on lifetime. However, it also leads to surface notches and tensile residual stresses in the bulk material with a negative impact on cyclic lifetime. During fully reversed uniaxial tension-compression fatigue tests (R = −1) at a stress amplitude of 260 MPa, the positive effects dominate, and the fatigue lifetime increases. At a lower stress amplitude of 230 MPa, the negative effect of internal tensile residual stresses dominates, and the lifetime decreases. Shot peening leads to a transition from surface to volume crack initiation if the surface is not damaged by the shots.

Keywords: shot peening; fatigue; gamma titanium aluminide; high temperature; residual stress; intermetallic

Citation: Breuner, C.; Guth, S.; Gall, E.; Swadźba, R.; Gibmeier, J.; Heilmaier, M. Influence of Shot Peening on the Isothermal Fatigue Behavior of the Gamma Titanium Aluminide Ti-48Al-2Cr-2Nb at 750 °C. *Metals* **2021**, *11*, 1083. https://doi.org/10.3390/met11071083

Academic Editor: Matteo Benedetti

Received: 28 May 2021
Accepted: 30 June 2021
Published: 6 July 2021

1. Introduction

Intermetallic gamma titanium aluminides (γ-TiAl) show excellent (weight) specific mechanical properties and good oxidation resistance even at high temperatures. For these reasons, they have been investigated since the 1970s [1]. An overview of the early alloy development can be found in [2]. Twenty years later, Appel et al. summarized the most important aspects of γ-TiAl alloys for engineering applications [3]. Due to their properties, γ-TiAl alloys are promising candidates to replace the higher density nickel-based superalloys in high-temperature applications, e.g., in turbine blades, turbochargers, or exhaust valves, at least for a temperature up to 800 °C. One of the commonly applied alloys is the second-generation alloy Ti-48Al-2Nb-2Cr (at.-%) (hereinafter referred to as 48-2-2) [2], which is used in the new LEAP engines by SNECMA [4], leading to a significant weight reduction in the LPT blades [5]. In service, turbine blades endure creep and fatigue loading, which typically determine their lifetime. While the isothermal and thermo-mechanical fatigue properties of TiAl alloys have been studied several times, see, e.g., [6–12], little attention has been paid to the possibilities of mechanical surface treatments such as shot peening to possibly achieve higher cyclic lifetimes.

Shot peening is a well-known method to increase the fatigue resistance of engineering materials, particularly of steels. Shot peening induces compressive residual stresses and leads to work hardening in the near-surface region [13]. The compressive residual stresses

locally reduce the effective maximum stress at the surface, which may delay or even inhibit crack initiation. The work hardening effect of the surface also improves the resistance against crack initiation and propagation. Fatigue cracks typically initiate at the surface [14], and it is known that shot peening can shift the crack initiation into the volume [15]. For volume cracks, the environmental influence on crack propagation is suppressed [16,17]; thus, an increase in cyclic lifetime can be expected. A strong dependence of the fatigue lifetime on the crack initiation site was reported in [7]. The effect of shot peening on the room temperature fatigue behavior of different γ-TiAl alloys was the subject in several publications, e.g., [15,18], and it is found that shot peening can improve the fatigue resistance for this class of material.

A further effect of shot peening is that the shot impacts create a higher surface roughness, which may contribute to better adhesion of surface coatings that are usually applied to reduce oxidation [19]. As a downside, shot peening typically roughens the surface, which may promote crack initiation due to locally increased stresses caused by the notch effect [20,21].

As γ-TiAl alloys are typically used at high temperatures, it must be considered that compressive residual stresses generated by shot peening may degrade due to stress relaxation during service operation [22,23]. In room temperature fatigue tests of shot-peened γ-TiAl alloys, which were long-term annealed at 700 °C prior to testing, it was found that the beneficial effects of compressive residual stresses on lifetime decreased due to stress relaxation [21].

To the authors' knowledge, how shot peening influences the fatigue behavior of γ-TiAl alloys at high temperatures has not been investigated yet. It can be expected that fatigue damage mechanisms and stress relaxation occur simultaneously, and it is not clear whether shot peening has an effect on lifetime. Further, while the compressive residual stresses at the surface may suppress surface crack initiation, the usually brittle surface oxide layers formed during exposure to high temperatures may promote it. Since high-temperature fatigue loading is highly relevant for shot-peened γ-TiAl components under service conditions, it is of crucial importance to understand the influence of shot peening on the damage mechanisms and lifetime.

Therefore, the present study considers the influence of shot-peening treatment on the isothermal high-temperature fatigue behavior of the γ-TiAl alloy 48-2-2. With regard to the possible benefit of a subsequently applied coating, a testing temperature of 750 °C was chosen, which is about 100 K higher than the recent application temperature. The objective is to provide a better understanding about if and how shot-peening processes can improve high-temperature fatigue lifetimes of γ-TiAl alloys, as well as a possible subsequently applied oxidation protective coating [19].

For that purpose, fully reversed compression–tension tests of untreated and shot-peened samples were conducted at 750 °C in the high cycle fatigue (HCF) regime. The result of the shot peening process was characterized using EBSD, microhardness, and residual stress analyses. To determine the effect of potential residual stress relaxation due to the thermal loading, shot-peened samples were annealed for 8 h at 750 °C, and results were compared with results for non-annealed samples.

2. Materials and Methods

The investigated material is the second-generation γ-TiAl alloy Ti-48Al-2Cr-2Nb (48-2-2) with a relatively coarse duplex microstructure, as shown in Figure 1. It consists mainly of γ phase with small amounts of α_2 phase and β phase. The rather coarse γ lamellae are separated by very thin α_2 lamellae. Within the γ grains, many twins are visible. The material was provided by GfE Nürnberg, Germany, and was produced by centrifugal casting. After casting, it was hot isostatically pressed (HIP) for 4 h at 1200 °C and 190 MPa to close porosity and contribute to chemical homogenization of the cylindrical rod with a diameter of ~80 mm. Optical microscopy with ensuing image analysis indicated that the microstructure was relatively coarse with an average grain size of approximately 80 µm.

The chemical composition is listed in Table 1. From the rods, smaller rods were sectioned by electro discharge machining (EDM). The geometry of the fatigue samples was first produced by turning. Since, for this material, the turning process induced small cracks with a crack length up to about 70 µm in depth, a layer of at least 200 µm was removed by grinding with a diamond tool until the final geometry was reached. Then, the gauge section was finished using sandpaper up to a grit size of 1000 to reduce the surface roughness.

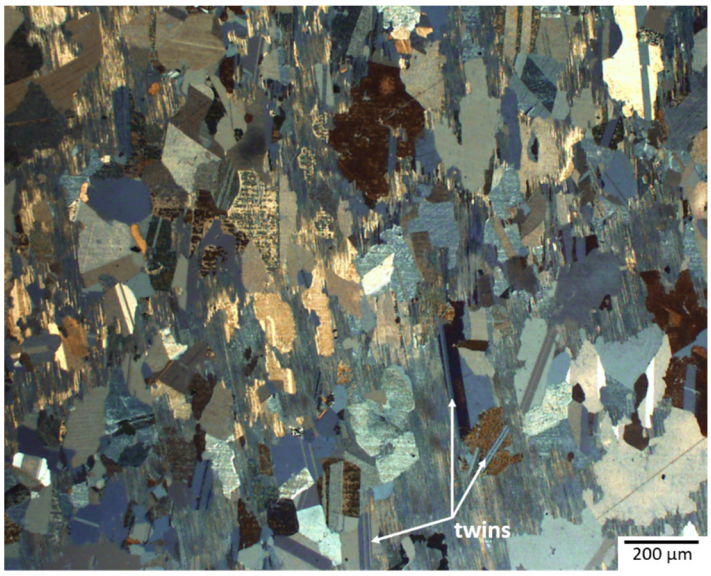

Figure 1. Light optical microscopy image of the microstructure of the investigated material after etching with Weck reagent (100 mL distilled water, 50 mL ethanol (96%), and 5 g ammonium-bifluorid [24]) using polarized light.

Table 1. Chemical composition (at.-%) of the TiAl alloy, measured with an Agilent 5100 ICP-OES.

Ti	Al	Cr	Nb
50.9	44.5	2.2	2.4

The shot peening (SP) was performed using a BAIKER industrial compressed air shot peening machine. Preliminary tests showed that round cast steel shots (S110) with an average diameter of 300 µm offer the best compromise between work hardening and surface quality. The intensity was chosen to an Almen intensity of 0.4 mmA with a coverage of approximately 300%.

The electron backscatter diffraction (EBSD) investigations were performed using a Field Emission Gun (FEG) Scanning Electron Microscope (SEM) JEOL JSM 7200F, operating at 15 kV accelerating voltage and equipped with a Hikari Plus EBSD detector by EDAX. The samples for EBSD analysis were coin-shaped and prepared by electropolishing using a Struers TenuPol-5 device and an A2 solution by Struers. To characterize the changes in the sub-surface microstructure of the studied materials, two types of EBSD maps were used: Image Quality (IQ) and Kernel Average Misorientation (KAM). The latter (KAM) is a measure of local grain misorientation. The contrast in IQ maps is sensitive to the presence of various phases, strain, and grain boundaries, whereas misorientation parameters of EBSD, such as KAM, can be used as a qualitative measure of deformation-induced changes in the microstructure of alloys. KAM has already been demonstrated to be a useful tool for characterization of deformation processes in TiAl alloys [25,26] and the shot peening effect on the surface microstructure of Ni-base superalloys [27,28].

To evaluate the effects of work hardening due to shot peening, microhardness profiles were measured on cross-sections using a Vickers-type micro-hardness tester, Qness Q10

A+, with an indentation load of 0.1 kg (HV 0.1). The micro-hardness was measured on cross-sections, which were ground with a diamond suspension up to 3 µm.

Residual stresses were determined by X-ray stress analysis (XSA) according to the $\sin^2\psi$ method [29] using Ni-filtered CuKα radiation. For the primary aperture, a ø 1 mm pinhole collimator was used. On the secondary side, a 2 mm slit was used in front of the scintillation counter. Seventeen sample tilts between $-60° \leq \psi \leq 60°$ were considered, which were equidistantly distributed in $\sin^2\psi$. From the γ-TiAl {204}/{312} reflections, the stronger {312}-diffraction line was separated by a Pearson VII multi-peak fit and used for stress determination. For the stress calculation, the diffraction elastic constants $E_{\{312\}}$ = 171 GPa and $\nu_{\{312\}}$ = 0.25 were used. Residual stress depth profiles were determined by a combination of a stepwise electrochemical layer removal and the reapplication of the $\sin^2\psi$-analysis on the newly generated surfaces. To validate the X-ray residual stress analyses on the relatively coarse-grained material, the incremental hole-drilling method was applied. Here, a drilling device of type RS-200 from Vishay Measurements Group and TiN-coated ø 0.8 mm milling tools were used. The strain relaxations were recorded using strain gauge rosettes of type EA-06-031RE-120 from the Vishay Measurements group. Stress evaluation was carried out using a differential approach and the elastic constants of E = 156 GPa and ν = 0.25.

The fatigue experiments were conducted on untreated and shot-peened samples under stress-controlled push–pull loading at 750 °C in laboratory air on a Schenck servo-hydraulic testing machine with 100 kN load capacity. The heating was achieved by an induction system. The test frequency was 5 Hz, and a load ratio of $R = -1$ (fully reversed) was applied. The maximum cycle number was set to 2×10^6, after which tests were stopped and counted as runout. For statistical analysis of lifetimes, a Weibull distribution was assumed. The characteristic lifetime was calculated at the 63.2 percentile according to Weibull. The form factor, which represents the slope of the Weibull approximation, is a measure of the scatter in a lifetime. A larger form factor indicates a smaller scatter.

To investigate the effect of residual stress relaxation, SP samples were annealed (SP+A) for 8 h at 750 °C, which equals the fatigue testing temperature. The annealing time corresponds to 144,000 fatigue cycles, which is approximately the mean lifetime of the material at about 290 MPa. After annealing, the microhardness and the residual stresses were analyzed again. No fatigue tests were performed on SP+A samples.

3. Results and Discussion

3.1. EBSD Analysis

The EBSD analysis depicted in Figure 2a–f compares the untreated material to the SP and the SP+A states. As shown in Figure 2a, the cross-sectional microstructure of the untreated TiAl alloy was composed of the large γ-TiAl grains (see also Figure 1) without any visible deformation except for the region very close to the surface, which is a preparation artefact. The corresponding KAM map, shown in Figure 2b, indicated a relatively strain-free microstructure on the microscopic scale, with a very thin surface layer of about 5 µm thickness characterized by elevated KAM values of around 1–2°. In the case of the SP sample, the IQ map (Figure 2c) revealed numerous slip bands in all grains located in the investigated region. Their amount gradually decreased inward towards the specimen, which agrees with the KAM map (Figure 2d) that revealed the presence of highly deformed grains in the sub-surface region, with the majority of KAM values being in the range of 1–3° (green and yellow colors) and some occasional areas reaching KAM values of 3–5° (red and dark colors). In the case of the SP+A sample, the presence of slip bands was less pronounced in the IQ map (Figure 2e) compared to the sample which was not annealed. Moreover, the KAM map indicated that there were no regions with KAM values of 4–5° (black color), whereas the number of the regions with KAM values of 3–4° (red color) was significantly reduced. However, in the major part of the sub-surface layer, the KAM values were around 1–2°. Additionally, it seems as if the increased KAM values were present at a higher depth compared to the SP samples; however, these are most likely lamellar colonies

containing not only the γ-TiAl, but also the α_2 phase. No significant grain refinement or recrystallization could be detected for SP and SP+A states.

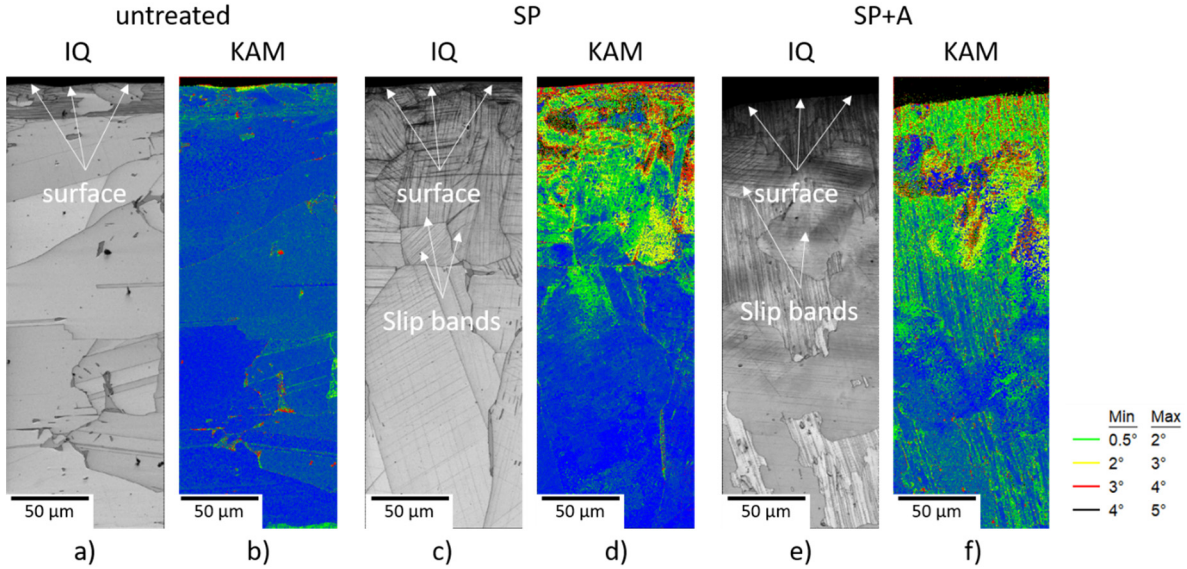

Figure 2. EBSD Image Quality (IQ) and Kernel Average Misorientation (KAM) maps of (**a**,**b**) untreated material, (**c**,**d**) SP material, and (**e**,**f**) SP+A material.

3.2. Micro Hardness

Figure 3 shows the hardness profiles for SP and SP+A samples, respectively. To determine the hardness depth profile, for every depth level a mean value was calculated out of at least six measurements. The error bars indicate the standard deviation. For both material states, the hardness increased towards the surface, and the maximum hardness occurred at about 60 µm below the surface. In the near-surface region, the hardness values of the annealed samples were lower than for the non-annealed samples. For depths greater than about 300 µm, the hardness values of both states were nearly identical and approached those of the base material. The transition between increased hardness and the hardness of the base material correlated well with the measured zero-crossing of the residual stresses (see later Figure 5), and the IQ measurement showed dislocations even at a depth of 300 µm.

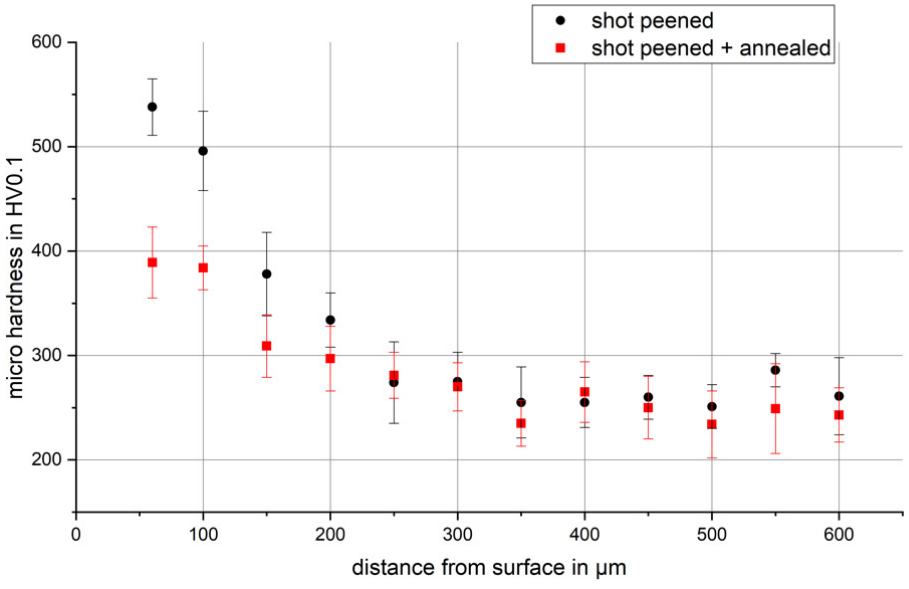

Figure 3. Hardness over distance from the surface.

3.3. Residual Stresses

Figure 4 shows the residual stress depth profiles for SP as well as for SP+A specimen and the mean integral width of the diffraction lines. For comparative studies using identical measuring conditions, the integral width of the diffraction lines can be taken as a qualitative measure to assess the degree of work hardening, since its changes are mainly based on changes of the density of lattice imperfections; hence, it correlates with the dislocation density. The highest compressive residual stress was beyond −800 MPa and was found within the first 50 µm from the surface. This is about twice as high as the nominal ultimate tensile strength. However, the alloy 48-2-2 showed pronounced tension–compression asymmetry. To check the high-compressive stresses for plausibility, tension and compression tests were conducted at room temperature. Compression tests revealed that the offset yield strength was −800 MPa, approximately twice as high as the tensile yield strength with 300 MPa, which supported the residual stress results.

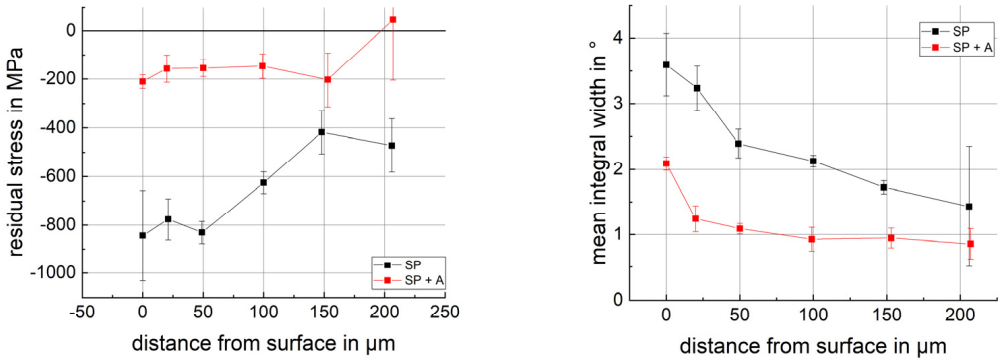

(**a**) (**b**)

Figure 4. Result of X-ray stress analysis: (**a**) Residual stress depth distributions for the SP and the SP+A samples and (**b**) the corresponding depth distributions of the mean integral widths of the diffraction lines.

The region of the compressive residual stresses exceeded a depth of 200 µm. However, for distances to the surface larger than 200 µm, it was not possible to measure residual stresses by XSA and the $\sin^2\psi$ method. This is due to the coarse microstructure, i.e., too few grains contributed to X-ray diffraction, resulting in poor statistics and unreliable results with an unacceptably high error. In the near-surface region, the shot peening caused a refinement of the microstructure, and XSA and the $\sin^2\psi$ method were very well applicable and resulted in reliable residual stress data.

The EBSD analyses confirmed the residual stress analyses by revealing a deep-reaching plastic deformation of the material after shot peening treatment. As can be seen in Figure 2, this led to a deformation-induced refinement of the microstructure near to the surface, which is a prerequisite to measure residual stresses with the $\sin^2\psi$ method with reasonable accuracy.

After annealing, the compressive residual stresses decreased considerably. In the region affected by shot-peening, they showed an almost homogeneous level of about −200 MPa. However, the compressive residual stresses were still in the order of the applied stress amplitudes in the fatigue tests.

The mean integral width of the diffraction lines depicted in Figure 4b implies that in the SP material there was a significant increase in the degree of work hardening induced by shot peening within the first 150 µm. After annealing, the mean integral width halves indicated that the dislocation density reduced due to recovery processes. This behavior correlated well with the microhardness distributions presented in Figure 3.

To determine the residual stresses at distances beyond 200 µm, an additional SP and an SP+A coin sample were analyzed using the incremental hole-drilling method, which is expected to be less sensitive to coarse grain effects. The residual stress distributions

determined by this means are displayed in Figure 5. In general, the results agree with the XSA results, i.e., high compressive residual stresses were determined in the near-surface region as a result of SP treatment. The stresses relaxed significantly after annealing at 750 °C. At the very near surface, the high compressive residual stresses of the SP treatment are overestimated by the hole-drilling method. This is a well-known effect that can be explained by plastic deformations in the vicinity of the hole, which affect the strain relaxations during stepwise drilling of the hole due to the notch effect of the blind hole [30]. However, apart from this overestimation, the residual stress distribution determined by this mechanical approach can be used for the assessment of the depth range beyond 200 µm. The data indicated that the zero-crossing of the residual stress distribution occurred at about 300 µm, and that in the bulk material balancing tensile residual stresses with a maximum of about 150 MPa occurred, even in the case of the annealed sample. Hence, these balancing tensile residual stresses must be considered for the assessment of fatigue testing.

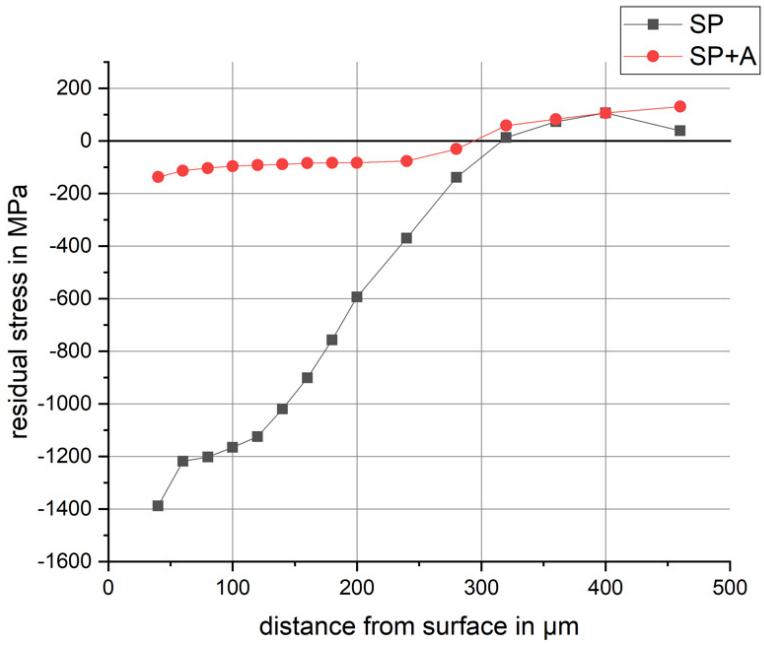

Figure 5. Residual stress depth distributions for the SP and SP+A samples determined using the incremental hole-drilling method.

3.4. Lifetime Results and Crack Initiation Behavior

Figure 6 compares the lifetimes of untreated and SP samples at 750 °C. The location of crack initiation for the particular samples is indicated. The lifetimes for a given stress amplitude fell in a scatter band of about a factor of 3.5. All untreated samples showed crack initiation from the surface. The lifetime of the SP samples at a stress amplitude of 260 MPa showed a bimodal lifetime distribution, i.e., depending on the crack initiation site lifetime was either short (surface) or long (volume), and the characteristic lifetime was slightly increased when compared to non-peened samples. When cracks initiated from the surface, the characteristic lifetime of the SP samples was reduced in comparison to untreated samples. These cracks initiated at larger notches caused by heavier shot impacts (see Figure 7a). All samples that failed from the surface showed only one crack initiation point. When cracks initiated in the bulk, the characteristic lifetime was higher than for untreated samples. When failing from the bulk, cracks initiated at several places before the final fracture occurred, see Figure 8.

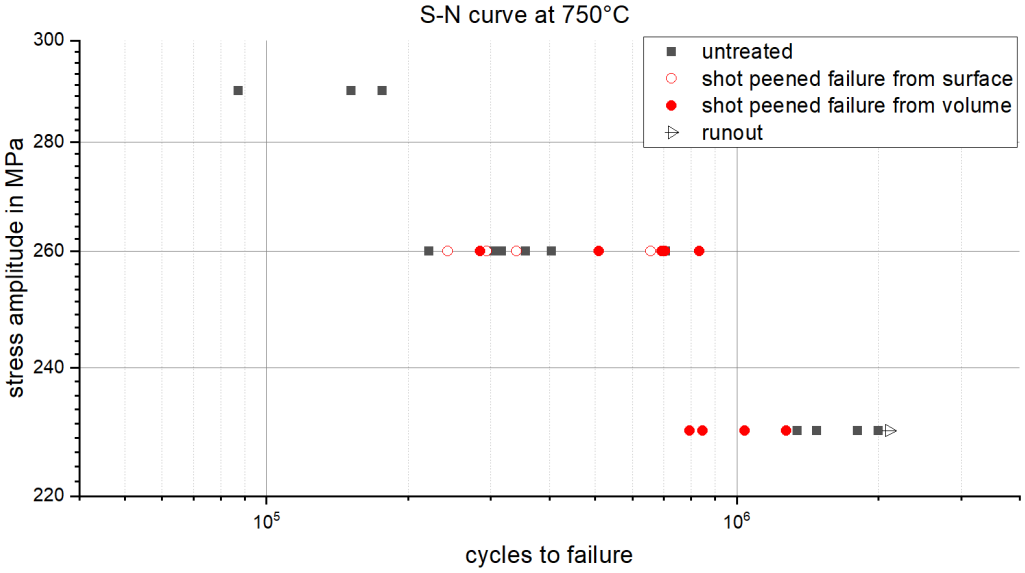

Figure 6. S-N diagram of the untreated and SP material at 750 °C showing a bimodal lifetime distribution at a load of 260 MPa.

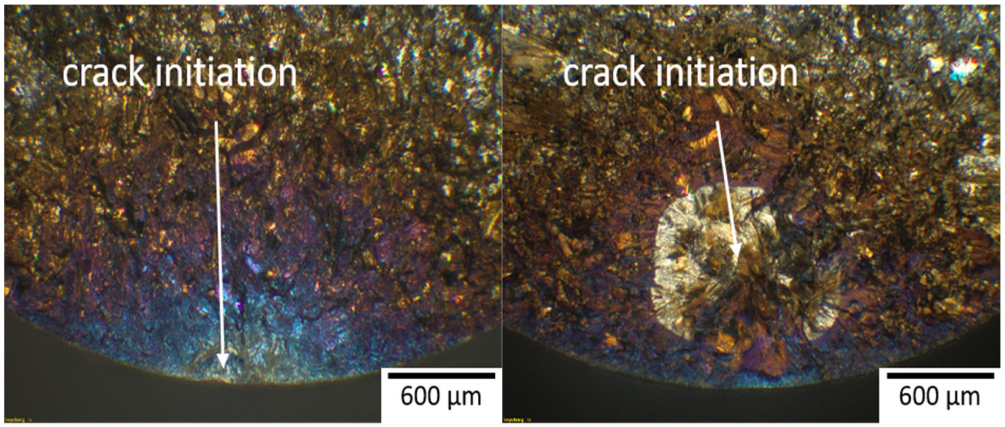

(**a**) (**b**)

Figure 7. Fracture surface of samples tested at 260 MPa. (**a**) Fracture surface after ~300,000 cycles with crack initiation from the surface starting at an impact and (**b**) fracture surface after ~500,000 cycles with crack initiation from the volume.

Thus, the observed distinct work hardening caused by shot peening delayed or prevented crack initiation at the surface. Furthermore, the compressive residual stresses could also prevent crack initiation or hinder small cracks from growing by locally reducing the effective tensile stresses. Both compressive residual stresses and the increased hardness after shot peening were reduced at the fatigue testing temperature of 750 °C (Figures 2–5). However, it was shown that even after 8 h at 750 °C, the compressive residual stresses of about −200 MPa were still on the order of the applied stress amplitudes, and the hardness near the surface was still about 50% higher when compared to the unpeened material state. Therefore, the combined effects may delay or suppress crack initiation from the surface and thus change the preferential crack initiation site from surface to volume.

The crack initiation from the surface was characterized by the oxidized area, which resulted in a colored fracture surface, also reported in [14]. The newly formed crack surface oxidizes, and depending on the oxidation time, different oxides or nitrides develop resulting in different colors. A yellow color indicates titanium nitride [31], and a grey color TiO_2 [32]. The different colors spread nearly semicircularly around the crack initiation point. The color also correlated with some microstructural characteristics. The light blue part

directly at the surface was quite flat and characterized by trans-granular crack propagation. An inter-granular crack propagation would be distinguishable by large facets due to the coarse microstructure. In the transition to the rather purple region, the fatigue fracture surface became rougher. The end of the bronze part indicated the transition to the final forced fracture of the sample.

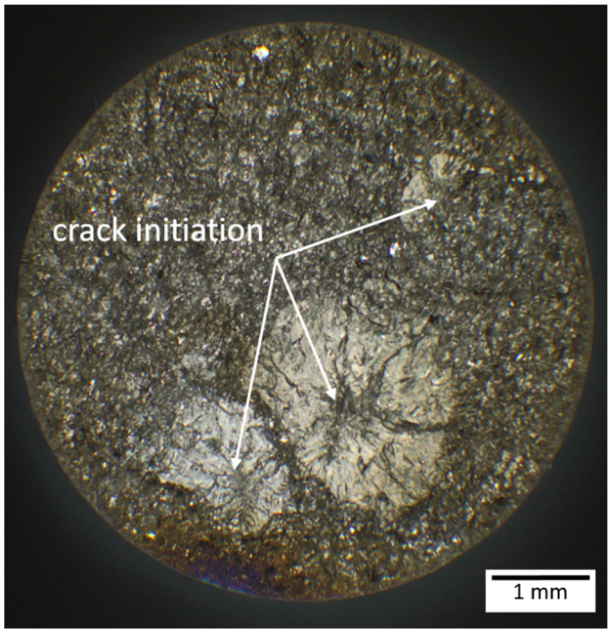

Figure 8. Fracture surface showing multi crack initiation in the volume of an SP sample fatigued at 230 MPa.

Cracks initiating from the volume spread circularly around their initiation point. The area of stable crack growth was characterized by trans-granular crack propagation. When initiating close to the surface, they broke through the surface and consequently grew as surface cracks. Contrary to crack initiation from the surface, multiple cracks grew in the volume at the same time until the final fracture occurred.

Hence, the change between the two crack initiation mechanisms produced the observed bimodal lifetime distribution. SP samples fail from the surface when they exhibit severe shot impacts. The negative effect due to the severe surface notches was compensated by the hardened surface and compressive residual stresses, which in the end led to no significant change in lifetime compared to the untreated material. The prolonged lifetime for specimens showing internal crack initiation may be explained by slower crack propagation in the bulk where the influence of the environment is negligible. It was shown by Mabru et al. that the crack propagation rate in γ-TiAl alloys was several magnitudes lower in vacuum than in air [16,17]. When the lifetime results at a stress amplitude of 260 MPa are separated according to the crack initiation location, the Weibull form factor, which is a measure for lifetime scatter, increased from 2.7 for all samples to 3.9 for the samples failing from the volume. This indicated that internal defects such as intrinsic notches or unfavorably oriented grains were rather homogeneously distributed in all specimens.

At a stress amplitude of 230 MPa, in contrast, shot peening reduced the lifetime slightly, though all SP samples failed from the volume. The bimodal distribution and the differences in the characteristic lifetime were analyzed in the following based on the assumption of a Weibull distribution [33].

Table 2 shows the characteristic lifetimes and form factors of the different conditions and loadings. A higher form factor indicates that the lifetime scatter is smaller. The untreated material revealed a characteristic lifetime of ~4.34×10^5 cycles and a form factor of 2.6 at a stress amplitude of 260 MPa. At this load level, the cracks always initiated at the

surface. One fracture surface with crack initiation from the surface can be seen in Figure 7a. At a stress amplitude of 230 MPa, the characteristic lifetime was about 1.77×10^6 cycles, and the form factor was 7.3. At this loading, one sample failed from the bulk and one test was a runout. The rest of the samples failed from the surface.

Table 2. Lifetimes of the different conditions and loadings.

	Characteristic Lifetime	Form Factor
260 MPa untreated	434,130	2.6
260 MPa shot-peened all	681,296	2.7
260 MPa shot-peened failed from surface	433,893	2.5
260 MPa shot-peened failed from volume	788,737	3.9
230 MPa untreated	1,769,659	7.3
230 MPa shot-peened all	1,069,388	5.6

The Weibull distribution of fatigue lifetimes of the SP samples at stress amplitudes of 260 MPa also revealed the bimodal distribution found in the S-N-diagram (Figure 6). The two failure mechanisms are considered separately, analogous to Jha et al. [7]. Crack initiation from the surface led to a lower characteristic lifetime of ~4.34×10^5 cycles. In comparison, samples with crack initiation in the volume showed a characteristic lifetime of about 7.89×10^5 cycles and, therefore, an increase of about 80% compared to the untreated material.

At a stress amplitude of 230 MPa, the lifetime of the SP samples was reduced by about 40% when compared to the untreated ones. All fatigue cracks initiated in the bulk, and no specimens failed from the surface. This indicated that, at this load level, the fatigue resistance of surface and volume were very similar. Contrary to 260 MPa, the shot-peening treatment reduced the fatigue lifetime, although all SP specimens showed crack initiation from the volume, which led to a lifetime increase at a stress amplitude of 260 MPa. One possible explanation for this unexpected behavior is the effects of subsurface tensile residual stresses developing during the fatigue and temperature loading, as reported in [15]. Results from the incremental hole-drilling method confirmed that tensile residual stresses were present at distances of about 400 µm below the surface. The tensile residual stresses after shot peening may have allowed volume cracks to initiate much earlier at unfavorably oriented grains or defects. Likely, the reduced crack propagation rate of internal cracks cannot compensate for this effect, and the overall lifetime is shorter.

To further investigate this unexpected behavior, additional samples were fatigued at 230 MPa and 260 MPa and stopped after 10^5 cycles (about half lifetime at 260 MPa) for both loadings and after 5×10^5 cycles (about half lifetime at 230 MPa) for the 230 MPa loading. Afterward, the residual stresses were analyzed by XSA at the surface. The residual stresses decreased to −20 MPa and −60 MPa, respectively, but were still present. Hence, it can be assumed that tensile residual stresses in the volume were still present. In addition, an in situ CT scan under tensile load was launched, and afterward, the specimens were then cracked completely to detect early induced internal fatigue cracks. However, these investigations did not reveal any early internal cracks. Further research is needed to study the influence of internal tensile residual stresses on crack initiation and propagation behavior.

Hence, the herein performed shot peening process can increase the fatigue resistance near the surface due to compressive residual stresses and work hardening as long as the shot impacts are not too severe. However, it decreases the volume fatigue resistance due to the build-up of tensile residual stresses.

It is assumed that for stress amplitudes lower than 230 MPa, volume crack initiation predominates, even in the untreated state. This means that a shot-peening treatment will presumably decrease the fatigue lifetime. Since low-stress amplitudes are most relevant for application, it can be concluded that shot peening is not a suitable treatment for γ-TiAl

48-2-2 under fatigue loading. When a shot-peening process is to be performed to prepare the surface for an oxidation protective coating, it should be as gentle as possible, i.e., moderate residual stresses and low surface roughness should be attained.

4. Conclusions

Stress-controlled fatigue experiments were conducted on shot-peened and untreated specimens of the γ-TiAl alloy 48-2-2 at 750 °C. From the results, the following conclusions can be drawn for the applied shot-peening parameters. For different parameters, these results may differ.

- Shot peening leads to high compressive residual stresses and increased surface hardness of the specimens due to work hardening. Stress-free annealing at 750 °C for 8 h reduces both effects; however, they are still significant.
- For untreated samples, fatigue cracks always initiated at the surface at a stress amplitude of 260 MPa, while for a stress amplitude of 230 MPa both internal and surface crack initiation occurred. Shot peening suppresses crack initiation from the surface and favors internal crack initiation.
- The lifetime of shot-peened samples showed a bimodal distribution at 260 MPa. The lifetime is comparable to the untreated material when cracks initiate at heavy shot impacts. The lifetime increased when the cracks started in the volume due to the strengthened surface.
- At a stress amplitude of 230 MPa, shot peening reduced the lifetime. This might be explained by the tensile residual stresses in the volume, which may lead to early volume crack initiation.

Author Contributions: Conceptualization, C.B. and S.G.; methodology, C.B.; investigation, C.B., E.G., J.G. and R.S.; writing—original draft preparation, C.B.; writing—review and editing, S.G., R.S., J.G., and M.H.; visualization, C.B.; supervision, S.G. and M.H. All authors have read and agreed to the published version of the manuscript.

Funding: This work was financially supported by the Deutsche Forschungsgemeinschaft (DFG) under grant LA 1038/13. The EBSD work was performed in the project Beethoven2 and funded by the National Science Centre, Poland, grant number UMO-2016/23/G/ST5/04128.

Institutional Review Board Statement: Not applicable.

Data Availability Statement: Not applicable.

Acknowledgments: The authors thank M. Zürn, F. Lang and P.T. Mai for the residual stress analyses, R. Rößler for technical assistance, and S. Dietrich (all from KIT) for scientific support.

Conflicts of Interest: The authors declare no conflict of interest.

References

1. Sastry, S.M.L.; Lipsitt, H.A. Fatigue deformation of TiAl base alloys. *Met. Mater. Trans. A* **1977**, *8*, 299–308. [CrossRef]
2. Kim, Y.-W. Ordered intermetallic alloys, part III: Gamma titanium aluminides. *JOM* **1994**, *46*, 30–39. [CrossRef]
3. Appel, F.; Paul, J.D.H.; Oehring, M. (Eds.) *Gamma Titanium Aluminide Alloys*; Wiley-VCH: Weinheim, Germany, 2009.
4. Bewlay, B.P.; Nag, S.; Suzuki, A.; Weimer, M.J. TiAl alloys in commercial aircraft engines. *Mater. High Temp.* **2016**, *33*, 549–559. [CrossRef]
5. Leyens, C.; Peters, M. *Titanium and Titanium Alloys: Fundamentals and Applications*; Wiley-VCH: Weinheim, Germany; John Wiley: Chichester, UK, 2003.
6. Roth, M.; Biermann, H. Thermo-mechanical fatigue behaviour of a modern γ-TiAl alloy. *Int. J. Fatigue* **2008**, *30*, 352–356. [CrossRef]
7. Jha, S.K.; Larsen, J.M.; Rosenberger, A.H. The Role of Competing Mechanisms in the Fatigue-Life Variability of a Titanium and Gamma-Tial Alloy. *JOM* **2005**, *57*, 50–54. [CrossRef]
8. Chan, K.S. The fatigue resistance of TiAl-based alloys. *JOM* **1997**, *49*, 53–58. [CrossRef]
9. Christ, H.-J.; Fischer, F.; Maier, H. High-temperature fatigue behavior of a near-γ titanium aluminide alloy under isothermal and thermo-mechanical conditions. *Mater. Sci. Eng. A* **2001**, *319–321*, 625–630. [CrossRef]
10. Christ, H.-J.; Fischer, F.O.R.; Schallow, P. Isothermal high-temperature fatigue behaviour of a near-γ titanium aluminide alloy. *Z. Met.* **2003**, *94*, 532–538. [CrossRef]

11. Heckel, T.K.; Christ, H.-J. Isothermal and thermomechanical fatigue of titanium alloys. *Procedia Eng.* **2010**, *2*, 845–854. [CrossRef]
12. Edwards, T. Recent progress in the high-cycle fatigue behaviour of γ-TiAl alloys. *Mater. Sci. Technol.* **2018**, *34*, 1919–1939. [CrossRef]
13. Almen, J.O. Shot blasting to increase fatigue resistance. *SAE Trans.* **1943**, *51*, 248–268. [CrossRef]
14. Planck, S.; Rosenberger, A. The influence of high temperature exposure on the mechanical performance of a γ titanium aluminide alloy. *Mater. Sci. Eng. A* **2002**, *325*, 270–280. [CrossRef]
15. Lindemann, J.; Buque, C.; Appel, F. Effect of shot peening on fatigue performance of a lamellar titanium aluminide alloy. *Acta Mater.* **2006**, *54*, 1155–1164. [CrossRef]
16. Mabru, C.; Henaff, G.; Petit, J. Environmental influence on fatigue crack propagation in TiAl alloys. *Intermetallics* **1997**, *5*, 355–360. [CrossRef]
17. Mabru, C.; Bertheau, D.; Pautrot, S.; Petit, J.; Henaff, G. Influence of temperature and environment on fatigue crack propagation in a TiAl-based alloy. *Eng. Fract. Mech.* **1999**, *64*, 23–47. [CrossRef]
18. Yang, Z.-J.; Sun, H.-L.; Huang, Z.-W.; Jiang, X.-S.; Chen, S. Fatigue properties of a medium-strength γ-TiAl alloy with different surface conditions. *Rare Met.* **2016**, *35*, 93–99. [CrossRef]
19. Madhavi, Y.; Krishna, L.R.; Narasaiah, N. Influence of micro arc oxidation coating thickness and prior shot peening on the fatigue behavior of 6061-T6 Al alloy. *Int. J. Fatigue* **2019**, *126*, 297–305. [CrossRef]
20. Sridhar, B.R.; Ramachandra, K.; Padmanabhan, K.A. Effect of shot peening on the fatigue and fracture behaviour of two titanium alloys. *J. Mater. Sci.* **1996**, *31*, 5953–5960. [CrossRef]
21. Huang, Z.; Lin, J.; Feng, B. Microstructural characterization and fatigue response of alloy Ti-46Al-5Nb-1W with varied surface quality and thermal exposure history. *Mater. Charact.* **2017**, *130*, 285–297. [CrossRef]
22. Vöhringer, O. Relaxation of residual stresses by annealing or mechanical treatment. *Residual Stresses* **1987**, 367–396. [CrossRef]
23. Schulze, V.; Burgahn, F.; Vöhringer, O.; Macherauch, E. Zum thermischen Abbau von Kugelstrahl-Eigenspannungen bei vergütetem 42 CrMo 4. *Mater. Werkst.* **1993**, *24*, 258–267. [CrossRef]
24. Petzow, G.; Carle, V. *Metallographisches, Keramographisches, Plastographisches Ätzen, Nachdr. der 6, vollst. Überarb*; Aufl. Borntraeger: Berlin, Germany, 2006; ISBN 978-3-443-23016-6.
25. Xiang, L.; Tang, B.; Xue, X.; Kou, H.; Li, J. Microstructural characteristics and dynamic recrystallization behavior of β-γ TiAl based alloy during high temperature deformation. *Intermetallics* **2018**, *97*, 52–57. [CrossRef]
26. Singh, V.; Mondal, C.; Sarkar, R.; Bhattacharjee, P.P.; Ghosal, P. Dynamic recrystallization of a β(B2)-Stabilized γ-TiAl based Ti–45Al–8Nb–2Cr-0.2B alloy: The contributions of constituent phases and Zener-Hollomon parameter modulated recrystalli-zation mechanisms. *J. Alloys Compd.* **2020**, *828*, 154386. [CrossRef]
27. Child, D.; West, G.; Thomson, R. Assessment of surface hardening effects from shot peening on a Ni-based alloy using electron backscatter diffraction techniques. *Acta Mater.* **2011**, *59*, 4825–4834. [CrossRef]
28. Messé, O.M.D.M.; Stekovic, S.; Hardy, M.C.; Rae, C.M.F. Characterization of Plastic Deformation Induced by Shot-Peening in a Ni-Base Superalloy. *JOM* **2014**, *66*, 2502–2515. [CrossRef]
29. Macherauch, E.; Müller, P. Das sin2ψ-Verfahren der röntgenographischen Spannungsermittlung. *Ztg. Angew. Phys.* **1961**, *7*, 305–312.
30. Gibmeier, J.; Nobre, J.P.; Scholtes, B. Residual Stress Determination by the Hole Drilling Method in the Case of Highly Stressed Surface Layers. *J. Soc. Mater. Sci. Jpn.* **2004**, *53*, 21–25. [CrossRef]
31. Becker, S.; Rahmel, A.; Schorr, M. Mechanism of isothermal oxidation of the intel-metallic TiAl and of TiAl alloys. *Oxid. Met.* **1992**, *38*, 425–464. [CrossRef]
32. Kofstad, P.; Hauffe, K.; Kjöllesdal, H.; Siekevitz, P.; Ernster, L.; Diczfalusy, E. Investigation on the Oxidation Mechanism of Titanium. *Acta Chem. Scand.* **1958**, *12*, 239–266. [CrossRef]
33. Biery, N.; De Graef, M.; Beuth, J.; Raban, R.; Elliott, A.; Pollock, T.M.; Austin, C. Use of weibull statistics to quantify property variability in TiAl alloys. *Met. Mater. Trans. A* **2002**, *33*, 3127–3136. [CrossRef]